Published version Digital Object Identifier 10.1109/JSENS.2018.2806564

Ranging RFID tags with ultrasound

Riccardo Carotenuto, *Member, IEEE*, Massimo Merenda, Demetrio Iero and Francesco G. Della Corte, *Senior Member, IEEE*

***Abstract*—Indoor localization and tracking of persons and assets with centimeter-level accuracy for inventory, security, medical monitoring and training, as well as gesture interfaces for domotics, is highly desirable in the framework of the emerging IoT paradigm. Low cost, tiny, battery or batteryless operated position sensors are required. 3D localization can be computed by combining three or more distance measurements between sensor and reference points. Our aim is to give the capability of measuring the distance from a reference point to RFID tags. The main challenge is in the estimation of the distances with millimeter accuracy in presence of both size and power supply strict constraints, and thus with very limited computational power. An accurate ranging technique using cross-correlation and small RFID-based sensors is proposed. Its originality resides in moving the main computational efforts from the sensor to an external processing unit with sufficient computational and supply power, thus overcoming the sensor limits. The system is composed of a beacon that emits ultrasound chirps and RF sync signals, a RFID-based distance sensor, a commercial RFID reader and a processing unit. Main advantages are the high miniaturization and low power consumption of the remote sensor, and its compatibility with existing RFID standards.**

***Index Terms*—ultrasound ranging, RFID tag, IoT smart devices ranging, ultrasound chirp, cross-correlation technique.**

I. Introduction

A NUMBER of high-speed mobile position-aware applications in several fields can be enabled by indoor localization systems with sufficient space and time resolution. They include IoT position-based applications, as well as human-machine gestural interfaces, virtual and augmented reality, domotics, medical monitoring and rehabilitation, flexible robotics, security access control, assets monitoring, and many others. Further applications cover safety, logistics, sport training, and gaming consoles. A localization system with sufficient resolution to distinguish fine movements of hands or limbs is required. A further desideratum is that the localization system should be minimally invasive and sufficiently low-cost. Small battery or batteryless operated sensors are highly desirable. Location can be determined by using Radio Frequency (RF) signals [1], sound waves [2], [3], magnetic fields [4] or optical signals [5]. Most of the positioning techniques require carrying out some distance measurements between reference points and a remote sensor. At least three distance measurements are required to localize a remote sensor in a semi-space using 3D trilateration.

Adding localization capability to existing RFID technology is very appealing [6], [7]. In fact, RFID technology has a readily available infrastructure, low-cost tags, and identification capabilities. Among the proposed techniques, RFID localization systems based on Received Signal Strength Indicator (RSSI) [8] are simple to realize but they are strongly affected by RF multi-path effects, with accuracy limited to meters. Reported systems [1] improve accuracy by using tags located in reference points and redundant readers. However, this increases system complexity, cost, and time spent for data analysis, which may be a challenge for the above-cited desired applications.

Ultrasonic waves are commonly used to measure the distance between an emitter and a receiver. Ultrasonic localization systems have been reported with higher accuracy than RF-based systems. In fact, it is easier to carry out time-of-flight (ToF) measurements on slowly propagating acoustic signals than to estimate distances using RF signals, typically relying on less accurate amplitude (RSSI) measurements. Ultrasound systems can use Time of Arrival (ToA), Time Difference of Arrival (TDoA) [2] or Angle of Arrival (AoA) [9], and localization accuracies on the order of centimeters have been reported. Ultrasonic distance measurement techniques can be based on ToF, or can include more sophisticated techniques as the single frequency continuous wave phase shift analysis, the combination of the ToF and phase-shift, the multi-frequency continuous wave and phase-shift, the multi-frequency amplitude-modulation and the binary frequency shift-keyed [10]–[13]. Moreover, several methods are based on digital signal processing, e.g. cross-correlation methods [14]–[18], and other techniques [19]–[26].

A key drawback of many existing acoustic systems is their power hunger, which results in wireless sensors with large batteries and weight as well as with short operating life. Moreover, severe constraints on size and power limit the computational power actually available onboard. Heavy computations are however required to apply the most accurate techniques such as cross-correlation. The battery issue can be partially overcome using RFID based system, in which the sensor is energized through the reading channel by the reading device [27], [28]. In [29], an RFID-based localization system was proposed using the custom passive Wireless Identification

Manuscript received October 25, 2017.

This work was supported by the MIUR [Project PON 03PE_00050_1 DOMUS SICUREZZA].

The authors are with the Mediterranea University of Reggio Calabria, Department of Information Engineering, Infrastructures and Sustainable Energy (DIIES), Via Graziella-Loc. Feo di Vito, 89122 Reggio Calabria, Italy (e-mail: r.carotenuto@unirc.it, massimo.merenda@unirc.it).

and Sensing Platform (WISP) platform. The system consists of a custom passive tag equipped with an acoustic tone-detector, which receives and times ultrasound signals, an off-the-shelf EPC Gen2 UHF RFID reader, and an array of ultrasonic beacons. By measuring the ToA of the ultrasound signals, the passive WISP tag can determine its location relative to the ultrasonic beacons. Time synchronization between the tag being tracked and the ultrasonic beacons is accomplished by using a "spy WISP" that listens to the RFID communication traffic between the reader and the tracked tag and triggers, in synchronicity with the RFID traffic, the ultrasound emission by the beacons. However, the low ToA time sampling, cadenced by the 32.768 kHz on board clock, seems to limit the ranging resolution to some centimeters. Additionally, both the variance of attenuation of the acoustic signal during propagation and the variations in the reported 25 kHz tone detection circuit affect the obtainable precision.

Cross-correlation based techniques allow ranging with superior accuracy compared to many other techniques. Unfortunately, cross-correlation is a power hunger algorithm not compatible with the severe power and size constraints of miniaturized RFID tags. The novelty of the proposed approach consists in moving the computational load from the sensor to an external processing unit, to which all the information required for the ranging is transferred through the RFID standard data channel. In this work, we add accurate ranging capabilities to RFID-based sensors by using a cross-correlation ranging technique. In this way, we exploit the high accuracy of ultrasound ranging and the best features of an RFID-based architecture, such as light weight, small size, unique identification of tags, as well as compatibility with existing RFID systems, yet using sensors with a minimal hardware.

Section 2 briefly provides motivation of the present work; Section 3 presents the ranging method in detail, while the architecture of the prototype system is described in Section 4. Section 5 presents experimental results and the characterization of the prototype. The prototype is capable of estimating the beacon-sensor distance of an RFID based sensor with an accuracy of few millimeters within a range of some meters, as required by most of the advanced indoor 3D localization applications above outlined.

II. Motivation

The method described in [29] exploits the best features of the standard RFID systems and the synchronization possibility offered by the standard communication protocol. On the other hand, it employs a simple tone detection circuit to estimate the ToA, while the ranging accuracy can be greatly improved exploiting a more sophisticated technique. The reported tone detector shows a noticeable dependence on signal amplitude and envelope shape in estimating the peak detection time, limiting the ranging resolution to several wavelengths. In fact, multipath distortion, i.e. reflections on obstacles and successive additive/destructive interferences between multiple delayed copies of the same travelling wave, could appreciably distort the shape of the received pulses. As a result, techniques based on simple threshold detection, or on identification of the signal envelope maximum, fail dramatically. Relevant ranging errors in the order of several wavelengths can be shown. As a further issue, the detection of the time-of-arrival of ultrasound tone bursts becomes very difficult or even impossible in presence of strong environmental acoustical noise or poor SNR.

Cross-correlation based methods show high accuracy and in general, good acoustical noise immunity. When using digital cross-correlation techniques, the acoustical signal is properly sampled and analog-to-digital converted. The resulting numerical samples' array R is cross-correlated with the digital reference signal S, previously stored in the memory. In more detail, considering that R and S are finite length arrays of real values and length N_R and N_S respectively, the m-th entry $c(m)$ of the cross-correlation $C = R \star S$ is given by:

$$c(m) = \sum_{n=1}^{N_S} R'(m+n-1)S(n), \qquad (1)$$

where $m = (1, 2, \ldots N_R+N_S-1)$ is the displacement or lag, and R' is the zero padded R, i.e. N_S -1 zeroes were added at the beginning and at the end of R before cross-correlating. It is well known that the maximum of the cross-correlation C indicates the point in time where R and S are best aligned. The cross-correlation peak lag is proportional to the ToF and, by assuming known the sound speed, to the distance between ultrasound emitter and receiver. It is worth noting that, differently from the envelope peak detection techniques, finding the cross-correlation peak allows for a distance estimation accuracy of the order of the current space sampling (i.e. the distance covered by the ultrasound during the time sampling interval), which is, in general, much smaller than the ultrasound wavelength. The key disadvantage using cross-correlation techniques is the massive processing, and thus the high-power levels required. Several commercial microprocessors are capable of carrying out the computations required by the cross-correlation technique within the given time constraints, but they in turn require a power supply of several tens of milliwatts during operation, which is not compatible with battery-less or even small battery-energized devices. As a consequence, the use of cross-correlation techniques on sensors equipped with small-size battery or even batteryless seems unfeasible.

III. Ranging Technique and System Architecture

A. The ranging technique

In this section, an innovative solution to some of the above-described ranging issues is proposed. Intensive cross-correlation computation is avoided onboard the sensor by moving most of it into an external Processing Unit, so that the advantages of cross-correlation are exploited without charging the sensor of the related computational burden.

This is achieved by employing the following technique. Briefly, a transducer placed at known coordinates emits a broadcast sync signal through its RF radio transmitter and an ultrasonic chirp.

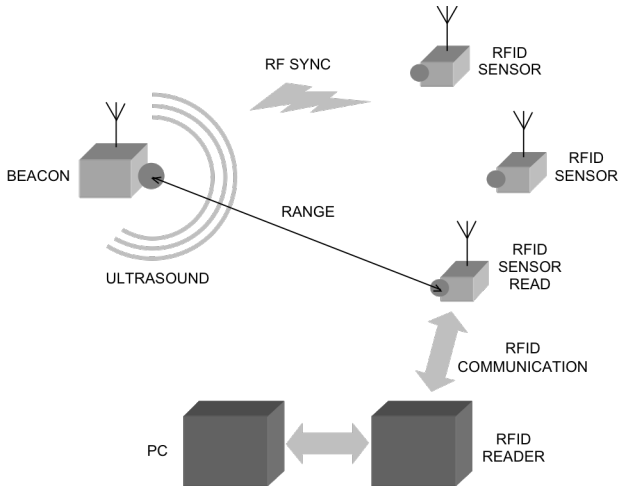

Fig. 1. Ultrasound ranging system architecture: ultrasound/RF beacon, multiple RFID-based range sensors, RFID reader and PC as Central Processing Unit.

All the sensors present in the ranging region, which receive the RF sync signal, start to receive and sample the ultrasound signal during the fixed receiving time window (whose duration depends on the maximum allowed range). At any time, a RFID reader can interrogate one of the sensors available, which it is seen by the reader as a usual RFID tag. This RFID sensor, instead of uploading to the reader only its EPC (or "identity"), also uploads the bits stored. They represent the sequence of the time sampled transitions of the received ultrasound chirp belonging to the last completed listening window. The reader then transmits these data to an external processing unit that reconstructs a "modified" version of the impinged chirp, cross-correlates it with the stored original chirp and computes its delay, from which it finally computes the range. The RFID protocol allows the reader to interrogate the RFID tags in its neighborhood only one at a time, and there is no limit to the number of RFID tags in a space region, other than the maximum number of possible EPCs used to code the identity of each tag (see Figure 1). In the following, a single sensor is considered.

More in detail, the ultrasound travels from the emitter to the sensor's microphone, where a suitable onboard circuit amplifies, filters and digitally squares the impinging ultrasonic signal. As a result, at the end of this chain, the impinging ultrasonic signal is converted into a sort of binary PWM signal [30]–[32]. Each low-to-high transition of such signal is accurately time sampled; the resulting time sequence data are stored onboard in the memory bank of a standard RFID tag. At any time, upon interrogation by the RFID reader unit, the content of the tag memory concerning the last completed ranging is transferred via a standard RFID protocol to the reader and then to a processing unit through a serial connection. A code running in the processing unit "restores" the PWM-like binary signal from the sequences of transition times received, and computes the cross-correlation with a previously stored copy of the emitted chirp. The cross-correlation peak lag is proportional to the ToF, and thus to the desired range estimate by assuming known sound speed. The

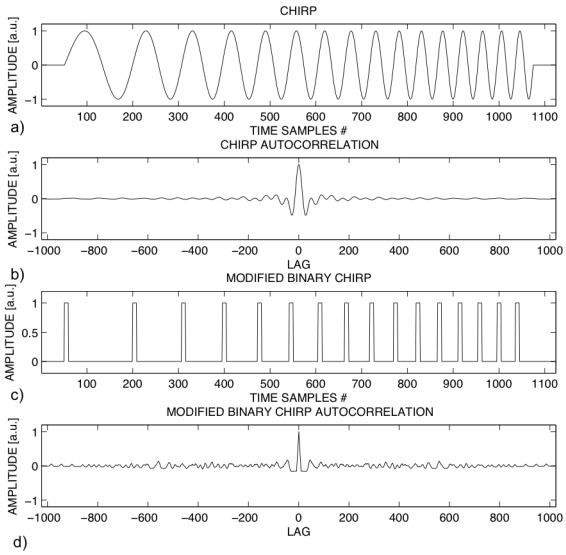

Fig. 2. Examples of: a) short chirp, c) modified binary chirp, and b), d) their autocorrelations (arbitrary units, a.u.). The sharp peak of the chirp autocorrelation is preserved in the MBS autocorrelation.

time resolution is given by the clock period that drives the timer onboard the sensor, while the length of the listening time window defines the ranging rate. The maximum repetition rate is limited by the time interval the sound takes to travel from the beacon to the farthest point of the actual ranging region.

The restored PWM-like signal, hereafter referred to as the "modified binary signal" (MBS), shows autocorrelation properties similar to the signal it is derived from. In particular, MBS presents the same cross-correlation peak displacement or lag of the original signal. It differs from the usual binary signal in the sense that the "1" signal duration is kept fixed and shorter than half the chirp pseudo-period. In Figure 2, a chirp and its derived MBS are showed and their autocorrelations compared. The MBS autocorrelation shows the typical triangular-shaped waveform of unipolar signals correlation. This triangular shape, a sort of bias that could interfere with the correct peak detection, is cancelled in Figure 2 by subtracting from one of the signals its own mean value before correlation.

B. System architecture

The ranging system architecture is described in the following (see Figure 3).

1) Ultrasound and RF beacon

The beacon emits periodically an ultrasound chirp and, at the same time, an RF synchronization signal. The beacon includes a microcontroller and a DAC, a power amplifier, an acoustic emitter, and an RF transmitter, in order to emit the chirp, stored in the microcontroller memory, and the synchronization RF signal.

When a set of distance measurements from different reference points is required for 3D localization, multiple beacons are deployed [30], [31]. In a 3D semispace, three distances from suitable reference points or beacons are sufficient to compute the sensor 3D location.

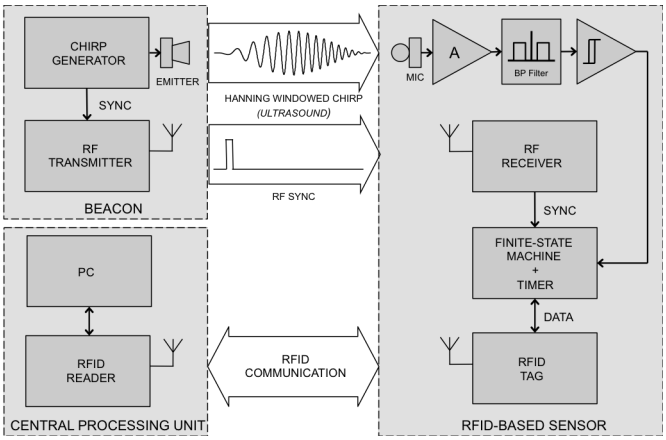

Fig. 3. Ultrasound ranging system functional diagram: ultrasound/RF beacon, RFID and PC (left), ultrasound and RF synchronization signals, RFID communication (center), and RFID-based range sensor (right).

These beacons are each other synchronized when emitting the same chirp in a given sequence, or are independent, but emitting uncorrelated chirps to avoid signal collision. Our envisaged system has such beacons mounted in the ceiling of the room where the system is intended to operate. For a convenient method of accurate localization of beacons after installation, see [33].

2) RFID-based sensor

The RFID-based sensor equipped with a microphone receives the impinging ultrasonic wave fronts. After a proper signal conditioning, the onboard finite-state machine, in correspondence of the low-to-high transitions of the squared incoming signal, reads a running timer and stores its content in a suitable memory bank. The running timer has been previously reset at the beginning of the listening window by RF synchronization signal, through the onboard RF receiver circuitry. At the end of the listening time window the timer data, stored in the memory bank, are immediately transferred into a standard RFID tag for a successive reading.

3) Central processing unit

The central processing unit (CPU) is composed of a standard RFID reader that downloads the timer data from the RFID tag sensor and of a processing device, for example a PC, a microprocessor board, or even a FPGA board, according to the requirements of the specific realization. The processing device receives the data from the RFID reader and, by means of a suitable code, restores the original MBS, cross-correlates the received MBS with a stored copy of the emitted ultrasound chirp signal, and displays the computed ranging data.

C. Sources of ranging uncertainty

The ToF and ranging estimation provided by the above system architecture is affected by some uncertainties. Provided that a suitable calibration procedure can estimate the fixed RF synchronization channel delay, still a not negligible time jitter is present; it mainly depends on the technology of the RF channel employed. A second source of uncertainty is, at the receiver side, the onboard timer granularity, which has its own clock period and an unavoidable drift. Moreover, the specific hardware realization of the finite-state machine that *i*) acknowledges the time of arrival of the squared waveform, *ii*) reads the internal timer content and *iii*) writes it in a memory bank, can introduce further time uncertainties. Air turbulence, unknown and inhomogeneous air temperature and humidity along the travelling wave path are further sources of inaccuracy.

D. Remarks

A drawback of all ToF techniques is that the peak associated with the true delay is not always the highest peak. In some cases, in fact, the straight-line (line-of-sight) path signal can be attenuated giving a lower peak than those of other signals coming from indirect paths. In other cases, a number of signals coming from indirect paths can combine to produce a higher peak than the one associated with the direct path signal. If the repetition time of the acoustic signal is correctly set, in respect to the environment characteristics, echoes from precedent emissions are sufficiently weak. Under this assumption, the first correlation peak above a certain threshold corresponds to the first received chirp, which traveled along the line of sight from the beacon to the sensor. Moreover, to prevent a misreading of the correct peak, a search mechanism can be applied to find the earliest arriving cross-correlation peak above the noise floor [34].

The proposed operating scheme shows remarkable advantages: 1) most of the computation effort and the energy need for accurately detecting the arrival time of the ultrasound signals are moved from the remote sensor to the CPU, since the cross-correlation computation is carried out entirely by the CPU. In this way, the sensor circuit complexity and power consumption are dramatically reduced. 2) The signal copies necessary for computing the cross-correlation don't reside on the remote sensor: when needed, the emitted signal can be dynamically changed to cope with acoustical disturbances or collisions, and different codes can be assigned to different ultrasound emitters without any change in the sensor hardware or firmware.

IV. System Realization

A. Prototype design choices

In order to use off-the-shelf components, the chirp frequency bandwidth has been chosen just beyond the upper frequency of the working bandwidth of commercial high quality microphones. A linear up-chirp in the bandwidth 15-40 kHz is employed. The sensor timer clock frequency is set to 1 MHz, so that the time resolution of the interrupt sampling is 1 μs. At this clock frequency, assuming the speed of sound in air 343 m/s, the space resolution is about 0.34 mm, which actually is the limit of the range estimation accuracy of this system. The chirp signal is composed of 1024 samples at 192 kSamples/s with a duration of about 5.33 ms, and it is Hanning windowed to avoid audible "clicking". An increased duration of the chirp improves the SNR of the cross-correlation, but at the expenses of both ranging rate and CPU computational effort. The components of the prototype are listed below.

B. Central Processing Unit

In this prototype, a PC is employed as the central processing unit of the system. However, a dedicated processor or FPGA could be used as well. Algorithms written in MATLAB (The MathWorks™, Natick, MA, USA) are executed on the PC in order to generate the acoustic signals that are emitted by the transducers, and to acquire, store and analyze the return data received from the remote sensor.

Signals are emitted by the MOTU 828 mk3 board (MOTU, Cambridge, MA, USA). This board provides ten analog inputs and ten analog outputs that can operate at a sample rate of up to 192 kSamples/s. However, the present prototype uses only two outputs of the board, one for the ultrasound emitter and the other for the RF transmitter of the beacon (see below). The connection with the PC is realized via FireWire.

An M6E MICRO UHF RFID reader (ThingMagic, Woburn, MA, USA) acquires the timer data from the tag section of the sensor and sends them to the PC via serial port.

C. Ultrasound and RF beacon

In the envisaged system, the beacon acts as independent periodic generator of ultrasound chirp and RF synchronization signal. However, in this prototype realization, for convenience, the ultrasound chirp and the RF synchronization are generated by the CPU through the MOTU 828 mk3 board. The ultrasound emitter employed is an HT 259 tweeter (CIARE S.r.l., Senigallia, AN, Italy), driven by a custom Class AB MOSFET power amplifier. Preliminary tests have shown that this specific model is able to emit sufficiently accurate chirp signals in the desired acoustic band. The transducer also has a reasonable low cost, in view of system mass production.

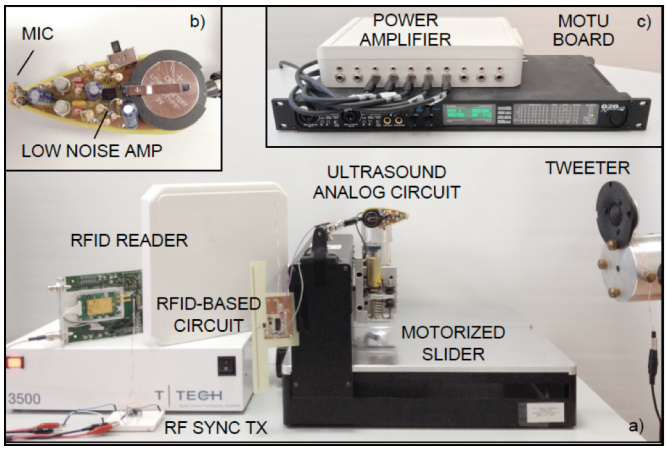

Fig. 4. System overview: a) RFID-based sensor including microphone, signal conditioning, and standard button type CR2032 lithium battery are hosted by a daughter board, while microcontroller and RFID tag are on the main sensor board; RFID reader antenna and circuit; RF transmitter; motorized slider and its controller; tweeter; b) analog circuit with miniaturized capacitive microphone and low noise amplifier; c) MOTU Board and Power Amplifier.

The RF transmitter is the TX section of an RTX MID 3V transceiver (Aurel S.p.A., Modigliana, FC, Italy), working at 433.92 MHz with binary ASK modulation scheme.

D. RFID-based remote sensor

The remote sensor is composed of an acoustical section for ultrasound signal sensing and conditioning, of a finite-state machine realized using a microcontroller for data sampling and storing, and of a RFID tag (see Figure 4).

The ultrasound circuit includes a miniature microphone FG-6163 (Knowles Acoustics, Itasca, Illinois, USA), which is a micromachined condenser microphone in a cylindrical shape package, length and diameter 2.6 mm, weight 80 mg, and acoustical receiving window diameter 0.79 mm. The receiving acoustical window is small compared to the used wavelength range (about 8.6-22.9 mm in the 15-40 kHz range, with sound speed in air 343 m/s), ensuring a good approximation of a point-like omnidirectional receiver.

The microphone is conditioned by a low-power circuitry including low noise pre-amplification and amplification stages (TLV2464, Texas Instruments, Texas, USA), a 15-40 kHz band-pass filter, followed by a Schmitt trigger in order to square the received signal, providing a two-level signal to the finite-state machine input. The RF receiver is the RX section of the RTX MID 3V transceiver (Aurel S.p.A. Modigliana, FC, Italy), working at 433.92 MHz with binary ASK modulation scheme. The onboard RF module works only in RX mode.

The finite-state machine is realized using a PIC18LF25K50 (Microchip Technology Inc., Chandler, AZ, USA). In particular, the firmware operates as follows: the decoded RF sync binary signal is fed to an interrupt pin (this is the sync interrupt) and resets two internal counters running at 1 MHz (see Fig. 5).

```
wait for SYNC SIGNAL
   reset ToF_Timer, reset listening_window_Timer
   if listening_window_Timer<Listening_window_duration
      wait for Incoming_Ultrasound_Transition_Interrupt
         t=read ToF_Timer, store t
      end
   end
   if Reader_upload_request
      upload to Reader
   end
end
```

Fig. 5. Finite state machine pseudo-code.

The digital output of the Schmitt trigger generated by each impinging ultrasound waveform transition causes a second interrupt (incoming ultrasound transition interrupt). At this time, the onboard state-machine reads the first counter value (t from the ToF_Timer) and stores it inside the PIC RAM. When the second counter (Listening_window_Timer) reaches a preset value (Listening_window_duration), which is related to the duration of the ranging operation, the interrupt from the incoming ultrasound signal is disabled and the content of the RAM is downloaded via serial connection to the onboard RFID tag user memory. Afterwards, upon RFID reader request, timer data are transferred through the RFID reader to

the processing unit for the above described processing. The sensor is then ready for the next ranging operation.

The RFID tag is a FRAM Embedded UHF Band RFID LSI FerVID family™ MB97R803A/B (Fujitsu Semiconductor Ltd., Yokohama, Japan).

The overall prototype remote sensor circuitry is powered by a standard button lithium battery type CR2032.

V. Experimental Results

A. Preliminary processing chain evaluation

The processing chain was preliminarily evaluated. During each ranging operation, the beacon emits a linear up-chirp from 15 to 40 kHz and the RF sync signal, at predefined time intervals. The RF sync triggers the interrupt of the PIC and two internal timers are reset. A calibration session estimated the time jitter of this operation being less than 1 μs, while the deterministic delay was 13.4 μs. The listening window was set to 12 ms, equivalent to a maximum range of about 4.11 m, assuming a speed of sound in air of 343 m/s. Figure 6 shows the details of the initial portion of the received experimental chirp, filtered and amplified by the wireless sensor circuitry (a); the modified binary chirp reconstructed in the processing unit using the timer data sequence downloaded from the RFID tag memory; c) the cross-correlation between the experimental restored MBS and the stored reference signal. The data displayed in Figure 6 were obtained with a sufficiently high SNR (30 dB) to test the full functionality of the complete processing chain. However, during regular operation in presence of environmental acoustical noise, the received modified binary signal shows a significant number of uncorrelated commutations, which in general decrease the amplitude of the cross-correlation peak, without however moving its position.

In the experiments that will follow, SNR decreases from about 35 dB at a range of 1 meter to 23 dB at a range of 3 meters, due to spherical spreading and air attenuation according to [35], where it is carried out an extensive power budget estimation for ultrasound localization systems.

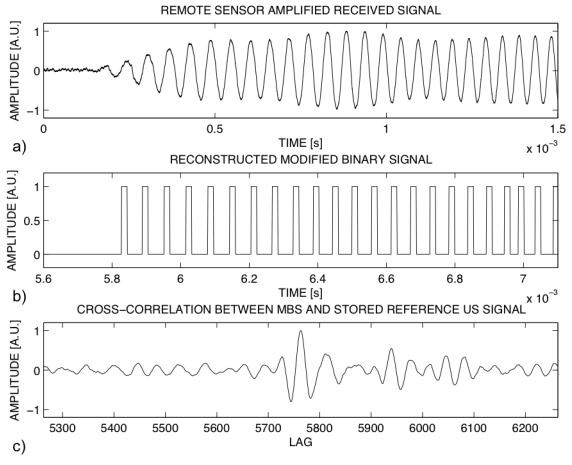

Fig. 6. Example zoomed portions of the experimental signals: a) chirp received, filtered and amplified by the sensor circuitry; b) modified binary chirp as restored in the processing unit from the timer data sequence from the RFID tag memory; c) cross correlation between the experimental restored MBS and the stored reference signal. The emitted signal is Hanning windowed to avoid audible "clicking".

A second calibration procedure estimated the time delay related to the timer reading of the ultrasound waveform transition interrupt in 14.3 μs with a time jitter of less than 1 μs. Finally, the time jitter of the sync signal on the RF channel was estimated in about 1.5 μs. The overall synchronization chain time jitter, which actually adds uncertainty to the ranging process, was experimentally estimated in about 3.7 μs (corresponding to a ranging uncertainty of about 1.3 mm), including the onboard clock drift. The actual ToF is obtained after a further calibration step, by comparing the measured distance between the beacon and the microphone with the computed one in order to compensate for other internal constant system processing delays. This procedure is required at the first use of the system only.

During the experiments, the sound velocity was assumed to be constant at 344.5 m/s (at measured room temperature $T_{room} = 21.8$ °C). The variation of sound velocity due to temperature and humidity were assumed to be negligible as the measurements were taken over a short period of time (e.g. when the temperature increases from 20 °C to 21 °C, the sound speed varies less than 0.2% or 4 mm over a 2 m range).

B. Accuracy and reliability remarks

The lower bound for the time accuracy detection of the time delay is given by the Cramér-Rao formulation [36]:

$$\sigma_D^2 \geq \frac{1}{16\pi^2 BTf_0^2 SNR}, \qquad (2)$$

where BT is time-bandwidth product, f_0 is the center frequency and SNR is the signal-to-noise ratio (SNR high enough to have no ambiguity in the peak detection). In the present case, $B = 25$ kHz, $T = 5.3$ ms, $f_0 = 27.5$ kHz, $SNR = 25$ dB, and $\sigma_D^2 \geq 1.31 \cdot 10^{-15}$ s. assuming the sound velocity 343 m/s at 20 °C, the distance error lower bound results about 12 μm.

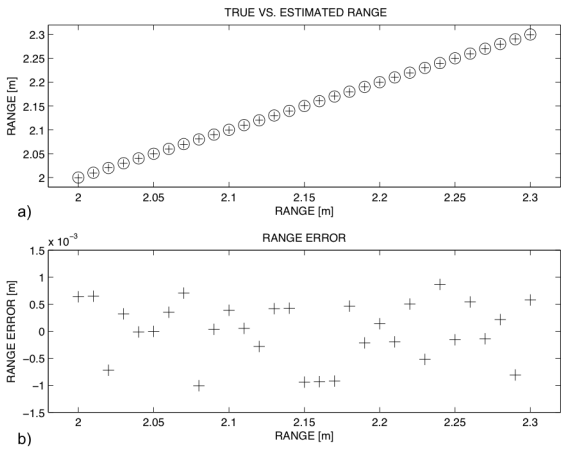

Fig. 7. a) Experimental ranging results (cross) compared to true distances (circle); b) range error.

However, we previously mentioned that the sensor samples onboard the ultrasound waveform transitions with 1 μs resolution. The time accuracy of the system is limited by its sampling rate and cannot be shorter than the duration of one clock period. The highest available range accuracy is therefore given by $p = vT_s$, where p is the accuracy margin in meters, v the sound speed and T_s the time between two successive samples. At 20 °C, this margin is equivalent to about 343 μm. Temporary strong acoustical disturbances and alterations in the sound speed due to humidity change, temperature drift and air mass flow, are other potential causes of wrong cross-correlation peak lag recognitions.

C. Experimental ranging results

The experimental ranging results and their errors, when the remote sensor is moved along a straight line, are shown in Figure 7. The analog ultrasound subsystem of the sensor is fixed to the x-axis slider of a motorized mill (Quick Circuit 5000S-E, T-Tech Inc. Norcross, GA, USA, resolution 1.2 μm, repeatability 8 μm) and connected to the main RFID-based subsystem through wires. We considered a ranging system operating in an average house or office room, where the emitter is placed on the ceiling geometrical center. For convenience, we set that the maximum range of this prototype is 2.3 m. In order to show the ranging performances in the worst conditions, the farthest 30 cm were analyzed, being 30 cm the allowed swing of the mill's slider. Nevertheless, if the system works well at the farthest portion of its range, it seems reasonable to assume *a fortiori* that it will work at any distance. The measurements are taken at steps of 1 cm along a straight line of length 30 cm, along the emitter axis. The line path starts from a point placed at 200 cm and stops at a distance of 230 cm from the emitter.

In order to be able to detect faulty measurements in the experiments and to evaluate the reliability of the proposed technique, each measurement was repeated 100 times. As a result, no abnormalities were measured and no outliers were eliminated. In consideration of the foreseen real-time use of the ranging system, where it is unpractical to average multiple measurements, in Figure 7 the experimental results of a single ranging operation are plotted. We arbitrarily took the 8th element for each slider position, from the set of 100 measurements for each position. The system ranges are in good agreement with the ones measured using the mechanical slider. Using the complete measurement data set (100 measurements per each range), the standard deviation was computed, which for all the 31 measured distances was below 0.7 mm (see Figure 8).

In Figure 9, the cumulative error distribution of the ranging data plotted in Figure 7 is shown, together with the cumulative error distribution of the data averaged over the 100 ranging operations for each slider position. The error is in good agreement with the estimated system time sampling and jitter limitations, and, as expected, the cumulative error distribution of the averaged data shows a better behavior.

Figure 10 shows the results of the 100 ranging operations at range 214 cm. It can be seen the typical value oscillation around an average value of the single measurements, which in the present case can be mainly ascribed to the timing jitter in the processor. The small drift of the data mean value seems to

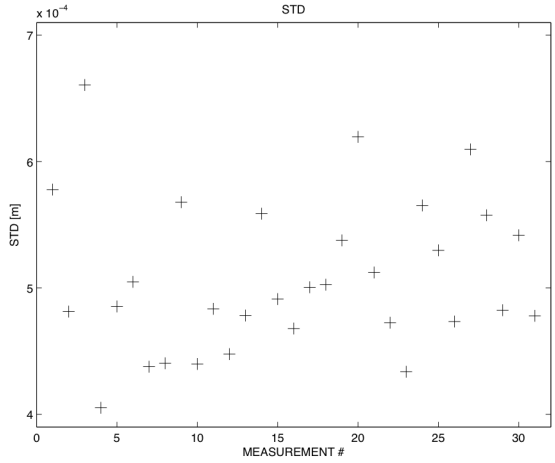

Fig. 8. Standard deviation of the 100 range measurements for each of the 31 positions of the slider from distance 200 cm to 230 cm.

be due to room temperature fluctuations during the measurements. The range values are quantized, and each range step is about 0.34 mm, according to the time granularity of the signal sampling process.

During operations, the measured average current provided by the battery was about 8 mA. It is worth noting that all the sensor circuitry, such as ultrasound microphone, analog

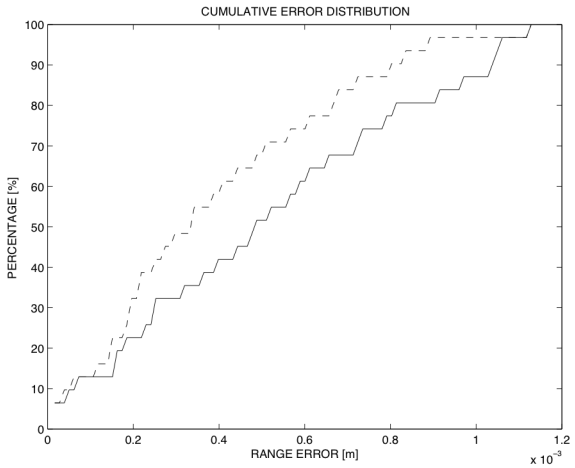

Fig. 9. Cumulative error distributions (percent of readings with error less than the value of a given abscissa) of the ranging data shown in Figure 7 (solid), and of the data averaged over the 100 ranging operations per distance (dashed).

conditioning, RF receiver, state-machine and RFID tag, could be easily realized using an ultra low power technology and designed as a single system-on-chip (SoC), which could be wireless powered using standard energy harvesting techniques. Ranging rate was about 1 Hz, limited by the RFID reading rate, which is the major bottleneck in our hardware setup. However, the focus of our work is actually on the possibility to add ranging capability to RFID tags using accurate cross-correlation techniques and existing communication standard

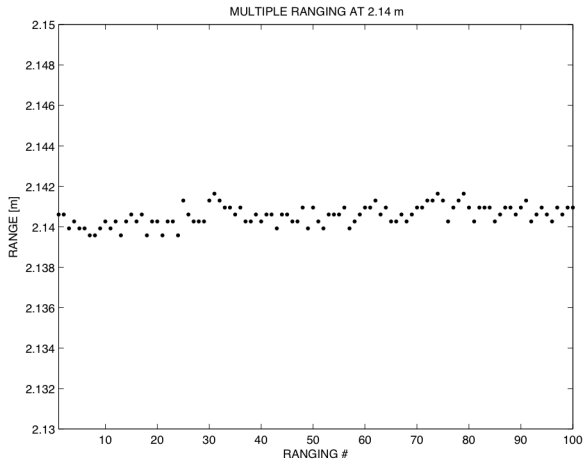

Fig. 10. Example of a typical sequence of range measurements at a given distance: 100 measurements at a distance of 2.14 m oscillating around a mean value; the oscillation is ascribed to the processing chain timing jitter. The small drift of the data mean value seems to be due to room temperature fluctuations during the measurements.

by moving the computation effort on a central unit. System performance optimization, as power consumption, ranging accuracy and rate, will be tackled in our future works.

VI. Conclusion

In this work, we presented a technique to move the computations related to accurate cross-correlation ranging from a RFID tag based sensor with minimal computational and power resources to and external processing unit, providing at the same time ranging accuracy in the order of millimeters, much smaller than the employed ultrasound wavelength. The major drawback of any cross-correlation technique is that it requires intensive computation, which cannot be executed on-board by a miniaturized battery-operated remote sensor. The proposed technique overcomes the sensor computational and power limits by moving the main computational efforts from the sensor to an external processing unit with sufficient power. Reasonably low ultrasound frequencies have been used, in order to use commercial and low cost ultrasound components, still obtaining millimeters ranging accuracy. Experimental results show a ranging accuracy of about ±1.2 mm within a range of 2.30 m. A ranging rate of 1 Hz has been achieved, actually limited by the standard RFID reading rate. The prototype ranging code runs on a standard PC notebook. The technique is fully compatible with existing RFID systems. The proposed technique potentially allows the realization of miniaturized ranging sensors as system-on-chip with small battery or even battery-free RFID reader powered. Very promising applications of the ranging method here proposed include, but are not limited to, IoT smart devices position-aware operation, gestural interfaces, domotics, real time tracking of human body movements, and gaming consoles. New coding schemes and processing algorithms will be investigated in the near future, in order to improve accuracy and remove the need of the RF sync signal.

References

[1] L. M. Ni, Y. Liu, Y. C. Lau, and A. P. Patil, "LANDMARC: Indoor Location Sensing Using Active RFID," *Springer Wirel. Networks*, vol. 10, no. 6, pp. 701–710, 2004.

[2] N. B. Priyantha, A. Chakraborty, and H. Balakrishnan, "The Cricket location-support system," in *Proceedings of the 6th annual international conference on Mobile computing and networking - MobiCom '00*, 2000, pp. 32–43.

[3] F. Ionescu, R. Carotenuto, and R. Urbani, "3D Localization and Tracking of Objects Using Miniature Microphones," *Wirel. Sens. Netw.*, vol. 3, no. 5, pp. 147–157, 2011.

[4] D. D. Arumugam, J. D. Griffin, and D. D. Stancil, "Experimental demonstration of complex image theory and application to position measurement," *IEEE Antennas Wirel. Propag. Lett.*, vol. 10, pp. 282–285, 2011.

[5] A. P. Sample, C. MacOmber, L. T. Jiang, and J. R. Smith, "Optical localization of passive UHF RFID tags with integrated LEDs," *2012 IEEE Int. Conf. RFID, RFID 2012*, pp. 116–123, 2012.

[6] T. Sanpechuda and L. Kovavisaruch, "A review of RFID localization: Applications and techniques," *5th Int. Conf. Electr. Eng. Comput. Telecommun. Inf. Technol. ECTI-CON 2008*, vol. 2, pp. 769–772, 2008.

[7] D. Zhang, F. Xia, Z. Yang, and L. Yao, "Localization Technologies for Indoor Human Tracking," in *IEEE Intl. Conf. on Future Information Technology (FutureTech)*, 2010, pp. 1–6.

[8] J. Torres-solis, T. H. Falk, and T. Chau, "A review of indoor localization technologies : towards navigational assistance for topographical disorientation," *Ambient Intell.*, pp. 51–84, 2010.

[9] M. Saad, C. J. Bleakley, T. Ballal, and S. Dobson, "High Accuracy Reference-free Ultrasonic Location Estimation," *IEEE Trans. Instrum. Meas.*, vol. 61, no. 6, pp. 1561–1570, 2012.

[10] F. J. Aldawi, A. P. Longstaff, S. Fletcher, P. Mather, and A. Myers, "A High Accuracy Ultrasound Distance Measurement System Using Binary Frequency Shift-Keyed Signal and Phase Detection," in *School of Computing and Engineering Researchers' Conference*, 2007, pp. 1–7.

[11] Y. P. Huang, J. S. Wang, K. N. Huang, C. T. Ho, J. D. Huang, and M. S. Young, "Envelope pulsed ultrasonic distance measurement system based upon amplitude modulation and phase modulation," *Rev. Sci. Instrum.*, vol. 78, no. 6, pp. 65103-65103–8, 2007.

[12] C. C. Tong, J. F. Figueroa, and E. Barbieri, "A method for short or long range time-of-flight measurements using phase-detection with an analog circuit," *IEEE Trans. Instrum. Meas.*, vol. 50, no. 5, pp. 1324–1328, 2001.

[13] S. S. Huang, C. F. Huang, K. N. Huang, and M. S. Young, "A high accuracy ultrasonic distance measurement system using binary frequency shift-keyed signal and phase detection," *Rev. Sci. Instrum.*, vol. 73, no. 10, p. 3671, 2002.

[14] K. Nakahira, S. Okuma, T. Kodama, and T. Furuhashi, "The Use of Binary Coded Frequency Shift Keyed Signals for Multiple User Sonar Ranging," in *IEEE Intl. Conf. Sensing and Control*, 2004, pp. 1271–1275.

[15] X. Zhao, Q. Luo, B. Han, and X. Li, "A novel ultrasonic ranging system based on the self-correlation of pseudo-random sequence," in *2009 IEEE International Conference on Information and Automation, ICIA 2009*, 2009, pp. 1124–1128.

[16] A. M. Sabatini and A. Rocchi, "Sampled baseband correlators for in-air ultrasonic rangefinders," *IEEE Trans. Ind. Electron.*, vol. 45, no. 2, pp. 341–350, 1998.

[17] A. M. Sabatini, "A stochastic model of the time-of-flight noise in airborne sonar ranging systems," *IEEE Trans. Ultrason. Ferroelectr. Freq. Control*, vol. 44, no. 3, pp. 606–614, 1997.

[18] A. M. Sabatini, "Correlation receivers using laguerre filter banks for modelling narrowband ultrasonic echoes and estimating their time-of-flights," *IEEE Trans. Ultrason. Ferroelectr. Freq. Control*, vol. 44, no. 6, pp. 1253–1263, 1997.

[19] K. Audenaert, H. Peremans, Y. Kawahara, and J. Van Campenhout, "Accurate ranging of multiple objects using ultrasonic sensors," in *Proceedings 1992 IEEE International Conference on Robotics and Automation*, 1992.

[20] M. M. Saad, C. J. Bleakley, and S. Dobson, "Robust high-accuracy ultrasonic range measurement system," *IEEE Trans. Instrum. Meas.*, vol. 60, no. 10, pp. 3334–3341, 2011.

[21] W. J. Cheng and F. R. Chang, "A novel ranging method by code and

multiple carriers of FHSS systems," in *Wireless Telecommunications Symposium*, 2012, pp. 1–6.
[22] Á. Hernandez *et al.*, "Ultrasonic ranging sensor using simultaneous emissions from different transducers," *IEEE Trans. Ultrason. Ferroelectr. Freq. Control*, vol. 51, no. 12, pp. 1660–1669, 2004.
[23] Y. Huang and M. Young, "An Accurate Ultrasonic Distance Measurement System with Self Temperature Compensation," *Instrum. Sci. Technol.*, vol. 37, no. 1, pp. 124–133, 2009.
[24] B. Barshan, "Fast processing techniques for accurate ultrasonic range measurements," *Meas. Sci. Technol.*, vol. 11, no. 1, pp. 45–50, 2000.
[25] D. Marioli, C. Narduzzi, C. Offelli, D. Petri, E. Sardini, and A. Taroni, "Digital Time-of-Flight Measurement for Ultrasonic Sensors," *IEEE Trans. Instrum. Meas.*, vol. 41, no. 1, pp. 93–97, 1992.
[26] J. R. Gonzalez and C. J. Bleakley, "Accuracy of spread spectrum techniques for ultrasonic indoor location," in *2007 15th International Conference on Digital Signal Processing, DSP 2007*, 2007, pp. 284–287.
[27] R. Berenguer, I. Rebollo, I. Zalbide, and I. Fernández, "Battery-less wireless sensors based on low power UHF RFID tags," *Wirelessly Powered Sens. Networks Comput. RFID*, pp. 79–109, 2013.
[28] R. Colella, L. Tarricone, and L. Catarinucci, "SPARTACUS: Self-Powered Augmented RFID Tag for Autonomous Computing and Ubiquitous Sensing," *IEEE Trans. Antennas Propag.*, vol. 63, no. 5, pp. 2272–2281, 2015.
[29] Y. Zhao and J. R. Smith, "A battery-free RFID-based indoor acoustic localization platform," in *2013 IEEE International Conference on RFID, RFID 2013*, 2013, pp. 110–117.
[30] R. Carotenuto and P. Tripodi, "Touchless 3D gestural interface using coded ultrasounds," in *IEEE International Ultrasonics Symposium, IUS*, 2012, pp. 146–149.
[31] R. Carotenuto, G. Caliano, and A. S. Savoia, "3D locating system for Augmented Reality glasses using coded ultrasound," in *IEEE International Ultrasonics Symposium, IUS*, 2013, pp. 441–444.
[32] R. Carotenuto, "A range estimation system using coded ultrasound," *Sensors Actuators, A Phys.*, vol. 238, pp. 104–111, 2016.
[33] A. Ens, L. M. Reindl, J. Bordoy, J. Wendeberg, and C. Schindelhauer, "Unsynchronized ultrasound system for TDOA localization," in *IPIN 2014 - 2014 International Conference on Indoor Positioning and Indoor Navigation*, 2014, pp. 601–610.
[34] L. Girod and D. Estrin, "Robust range estimation using acoustic and multimodal sensing," in *Proceedings 2001 IEEE/RSJ International Conference on Intelligent Robots and Systems. Expanding the Societal Role of Robotics in the the Next Millennium (Cat. No.01CH37180)*, 2001, vol. 3, no. FEBRUARY 2001, pp. 1312–1320.
[35] S. Holm, "Hybrid ultrasound-RFID indoor positioning: Combining the best of both worlds," in *2009 IEEE International Conference on RFID, RFID 2009*, 2009, pp. 155–162.
[36] A. Weiss and E. Weinstein, "Fundamental limitations in passive time delay estimation--Part I: Narrow-band systems," *IEEE Trans. Acoust.*, vol. 31, no. 2, pp. 472–486, 1983.

Riccardo Carotenuto (M'00) was born in Rome, Italy. He received the Dr. Sc. degree in Electronic Engineering from the University of Rome "La Sapienza", Rome, Italy. In 1997, he earned the Ph.D. degree from the University of Rome "La Sapienza", and joined the Department of Electronic Engineering, University Roma Tre, working on ultrasonic micromotors, on resolution enhancement of echographic imaging systems, and on theory and technology of capacitive micromachined ultrasound transducers. Since 2002, he has joined the Department IMET (now IIES), University "Mediterranea", Reggio Calabria, Italy, as Associate Professor. His main interests include indoor localization, ultrasound imaging, ultrasound actuators, time series prediction, nonlinear systems identification and control, neural networks theory and applications. Dr. Riccardo Carotenuto is author of more than 80 papers published on International Journals and Conferences Proceedings.

Massimo Merenda received the B.S., M.S., and Ph.D. degrees in electronic engineering from University "Mediterranea" of Reggio Calabria, Italy, in 2002, 2005 and 2009, respectively. From 2003 to 2005 he was a fellow at IMM-CNR, Naples, Italy. Since April 2011 he has been a temporary research associate in the DIIES department of "Mediterranea" University of Reggio Calabria. His research involved the design and development of application specific integrated circuits (ASIC), silicon sensors, embedded systems and intelligent radiofrequency identifiers (smart-RFID). Massimo Merenda was a recipient of the Prof. A. Rizzo Award from the Italian Sensor Association in 2007.

Demetrio Iero was born in Reggio Calabria, Italy, in 1982. He received the master's degree on Electronic Engineering, from the University "Mediterranea" of Reggio Calabria, Reggio Calabria, Italy in 2010, and PhD in 2014. He is a Temporary Research Associate in the DIIES department of the University "Mediterranea" of Reggio Calabria. His main research activities include power electronics and switching power loss measurement, microcrontrollers, IoT, and RFID plaftorms.

Francesco G. Della Corte (M'98, SM'15) was born in Naples, Italy. He received the M.S. degree in Electronic Engineerig from the *Federico II* University, Naples, Italy, in 1988. He was with Sirti spa, CNR-IMM, ENEA, Optel-InP. He is now a Full Professor of Electronics at the Mediterranea University of Reggio Calabria, Italy, serving as the Coordinator of the M.S. Progam in Electronic Engineering and head of the Microelectronics Lab. His main research topics are integrated sensors, wide bandgap semiconductor device modeling, silicon photonics, subjects on which he authored or co-authored more than 100 journal papers and holds 3 patents.